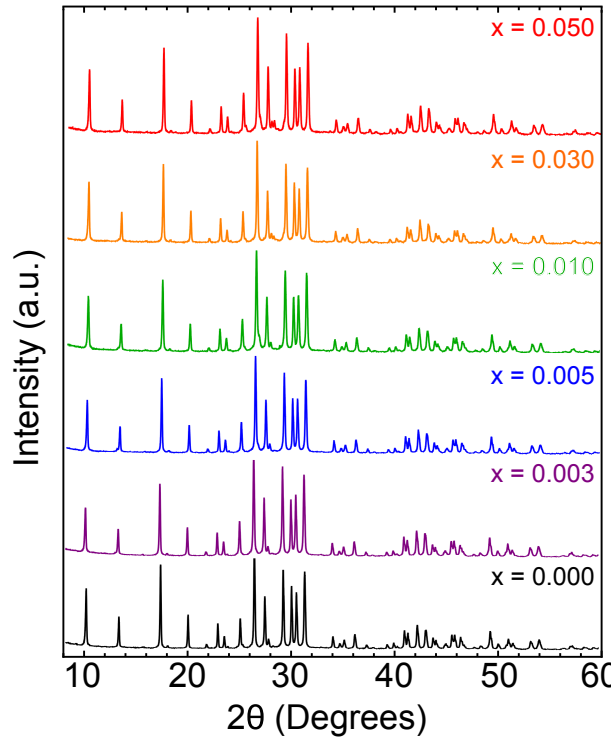


1 ELECTRONIC SUPPLEMENTARY INFORMATION

---

## 1 Electronic Supplementary Information

In this supplementary section, we provide additional structural and transport data to augment the results provided within the main body. Figure S1 provides all X-ray diffraction traces for samples used in the main body. Table S1 provides all the values used to generate the radar plot comparison between *p* and *n*-type Zintl materials. Figures S3, S2, and S4 provide additional data used in calculation of the lattice thermal conductivity. Figure S5 provides the  $zT$  predictions for  $\text{KAlSb}_4$  as a function of carrier concentration, within the single parabolic band model. Finally, Figure S6 shows the calculated density of states for  $\text{KAlSb}_4$ , decomposed into the contributions from individual atomic orbitals.



**Figure S1** X-ray diffraction patterns for Ba-doped and intrinsic  $\text{KAlSb}_4$ . Samples with  $x < 0.01$  Ba are  $>98\%$  phase pure, with a minor impurity phase too weak to be indexed. Samples with higher concentrations of barium also exhibit an additional impurity phase, whose intensity is too weak to be indexed. No appreciable shift in lattice parameters or volume are observed due to the low concentrations of barium and the similarities of the barium and potassium ionic radii.

**Table S1** Calculated transport properties for Zintl compounds with  $\beta > 10$ . We note that the promising *n*-type Zintl materials outnumbers the promising *p*-type materials by more than double. Data shown is a subset of the 145 calculations performed on a much more general dataset. Please note that all calculations are available (alongside >2000 other materials) on [www.tedesignlab.org](http://www.tedesignlab.org). We note that there are many antimonides and bismuthides that do not explicitly appear on the list due to the propensity of DFT to underestimate the band gap (yielding many antimonides and bismuthides as zero gap materials). However, we expect that many of the arsenide results will generalize to their antimonide and bismuthide analogues. PbTe is shown in both the *p* and *n*-type tables for reference. While the band degeneracies ( $N_p$ ,  $N_n$ ), and effective masses ( $m^*_{p,DOS}$ ,  $m^*_{n,DOS}$ ,  $m^*_{p,Band}$ ,  $m^*_{n,Band}$ ) are direct results from the first-principles DFT calculations, the thermal conductivity ( $\kappa_L$ ), mobility ( $\mu_p$ ,  $\mu_n$ ) and quality factor ( $\beta_p$ ,  $\beta_n$ ) are calculated using the semi-empirical model described in our prior work (Jun Yan et. al.).

***n*-type**

Compound	ICSD	$N_p$	$N_n$	$m^*_{p,DOS}$	$m^*_{n,DOS}$	$m^*_{p,Band}$	$m^*_{n,Band}$	$\kappa_L$	$\mu_p$	$\mu_n$	$\beta_p$	$\beta_n$
<b>PbTe</b>	<b>648608</b>	<b>4</b>	<b>4</b>	<b>0.213</b>	<b>0.169</b>	<b>0.197</b>	<b>0.643</b>	<b>6.09</b>	<b>188.21</b>	<b>265.80</b>	<b>13.37</b>	<b>15.35</b>
BaGa <sub>2</sub> As <sub>2</sub>	380378	3	8	2.19	1.99	1.05	0.50	3.25	4.05	12.47	3.93	16.41
SrSn <sub>2</sub> As <sub>2</sub>	611428	2	7	0.87	0.74	0.55	0.20	5.57	12.08	53.74	2.51	15.97
NaAs	182159	4	4	4.55	0.50	1.81	0.20	2.52	1.23	33.58	3.32	12.47
Na <sub>2</sub> CuAs	43937	1	4	0.56	0.42	0.56	0.17	3.63	8.60	51.79	1.40	11.50
Ca <sub>3</sub> In <sub>2</sub> As <sub>4</sub>	61336	1	1	0.24	0.02	0.24	0.02	4.43	44.36	1533.71	2.74	11.30
KCdAs	609963	2	1	1.97	0.02	1.24	0.02	3.11	2.24	1142.95	1.75	10.60
NaK <sub>2</sub> InAs <sub>2</sub>	300137	1	1	2.22	0.03	2.22	0.03	2.16	0.74	608.06	0.70	10.31
NaK <sub>2</sub> GaAs <sub>2</sub>	300129	1	1	4.12	0.03	4.12	0.03	2.16	0.29	606.91	0.48	10.20
Na <sub>2</sub> AuAs	23264	1	2	0.40	0.16	0.40	0.10	2.58	12.96	106.45	2.19	10.16
KSnSb	33933	2	7	0.53	0.06	0.33	0.02	2.49	12.76	1103.38	3.80	79.60
Mg <sub>3</sub> Sb <sub>2</sub>	642809	1	6	0.27	0.29	0.27	0.09	6.84	35.27	199.38	1.61	19.27
NaSb	26473	6	4	1.04	0.40	0.32	0.16	1.76	13.38	37.05	16.07	16.10
KGaSb <sub>4</sub>	300158	1	2	0.30	0.12	0.30	0.08	1.41	13.71	106.91	3.33	15.14
Rb <sub>3</sub> Au <sub>3</sub> Sb <sub>2</sub>	78978	5	4	2.09	0.66	0.71	0.26	1.13	2.94	13.25	9.58	14.00
RbSb	280591	3	4	2.95	0.62	1.42	0.25	0.95	0.84	11.67	3.61	13.80
KAlSb <sub>4</sub>	300157	1	2	0.26	0.14	0.26	0.09	1.51	17.66	94.39	3.49	13.63
K <sub>3</sub> Au <sub>3</sub> Sb <sub>2</sub>	78977	7	4	1.93	0.65	0.53	0.26	1.48	5.59	16.30	14.90	13.06
KSb	56529	3	4	3.23	0.60	1.55	0.24	1.23	0.85	14.12	3.09	12.66
CaCd <sub>2</sub> Sb <sub>2</sub>	12151	2	2	0.76	0.09	0.48	0.06	4.95	13.77	340.71	2.86	10.30
Ba <sub>3</sub> AlSb <sub>3</sub>	32728	3	3	0.81	0.47	0.39	0.23	2.58	14.94	33.44	7.41	10.23
Ba <sub>2</sub> GaBiS <sub>5</sub>	261677	4	6	7.91	1.24	3.14	0.30	2.06	0.23	20.91	0.84	20.33
Na <sub>2</sub> AuBi	261788	6	4	0.97	0.39	0.29	0.15	1.81	16.46	43.72	18.15	17.88
CsSiBiS <sub>4</sub>	281169	5	5	9.45	1.23	3.23	0.33	0.81	0.13	7.40	1.74	17.04
KMnBi	601586	2	1	2.61	0.03	1.64	0.03	2.00	1.11	506.02	1.70	10.00

***p*-type**

Compound	ICSD	$N_p$	$N_n$	$m^*_{p}$	$m^*_{n,DOS}$	$m^*_{p,Band}$	$m^*_{n,Band}$	$\kappa_L$	$\mu_p$	$\mu_n$	$\beta_p$	$\beta_n$
<b>PbTe</b>	<b>648608</b>	<b>4</b>	<b>4</b>	<b>0.213</b>	<b>0.169</b>	<b>0.197</b>	<b>0.643</b>	<b>6.09</b>	<b>188.21</b>	<b>265.80</b>	<b>13.37</b>	<b>15.35</b>
LiAsS <sub>2</sub>	419061	10	2	1.62	1.22	0.35	0.77	2.59	12.81	3.92	19.20	2.40
LiAsSe <sub>2</sub>	248116	8	2	2.48	1.79	0.62	1.13	1.87	4.79	1.96	13.30	2.30
NaSb	26473	6	4	1.04	0.40	0.32	0.16	1.76	13.38	37.05	16.07	16.10
K <sub>3</sub> Au <sub>3</sub> Sb <sub>2</sub>	78977	7	4	1.93	0.65	0.53	0.26	1.48	5.59	16.30	14.90	13.06
Na <sub>3</sub> K <sub>6</sub> AlSb <sub>4</sub>	401209	7	1	2.61	0.06	0.71	0.06	1.51	3.36	143.04	11.50	7.37
Na <sub>3</sub> K <sub>6</sub> GaSb <sub>4</sub>	77274	7	1	3.14	0.07	0.86	0.07	1.44	2.52	120.97	10.62	7.14
BaAgSb	56981	2	3	0.11	0.44	0.07	0.21	4.17	231.76	43.52	10.00	7.70
CsBiS <sub>2</sub>	72975	5	1	5.14	0.46	1.76	0.98	0.96	1.57	1.63	19.00	1.66
Na <sub>2</sub> AuBi	261788	6	4	0.97	0.39	0.29	0.15	1.81	16.46	43.72	18.15	17.88

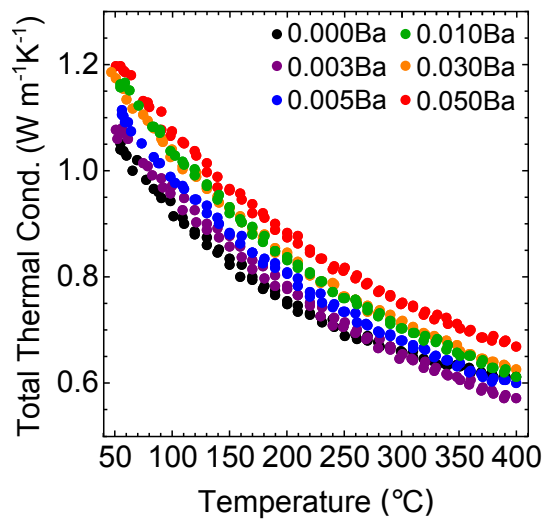


**Figure S2** Total thermal conductivity of Ba-doped  $\text{KAlSb}_4$  is quite low, consistent with a complex Zintl phase. Variation in the thermal conductivity with Ba-doping is largely attributed to the electronic contribution to the thermal conductivity resulting from increased carrier concentration.

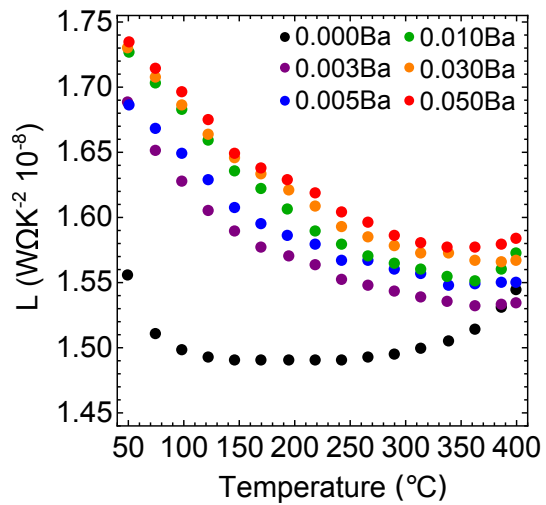


**Figure S3** Lorenz numbers for  $\text{KAlSb}_4$  calculated from the single parabolic band (SPB) model assuming acoustic phonon scattering as the primary scattering mechanism. Note that due to the activated transport at low temperatures ( $< 250^\circ\text{C}$ ), the low temperature Lorenz numbers are slightly less accurate.

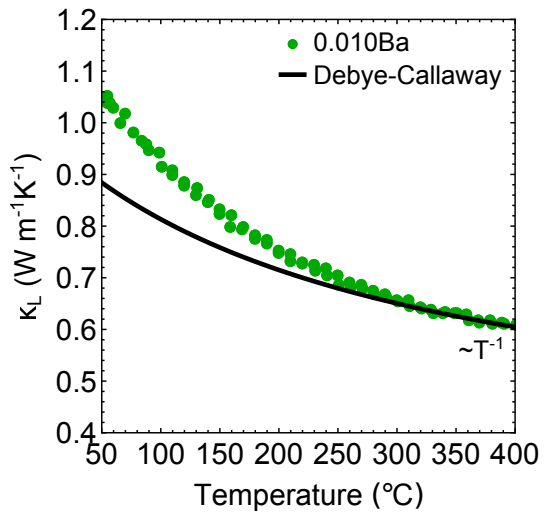


**Figure S4** The Debye-Callaway model reveals that the lattice thermal conductivity exhibits an approximate  $T^{-1}$  relationship (phonon-phonon scattering) at high temperatures but diverges at low temperatures. However, the Lorenz number used in the calculation of the lattice thermal conductivity may be less accurate at low temperatures due to the strongly activated electronic transport.

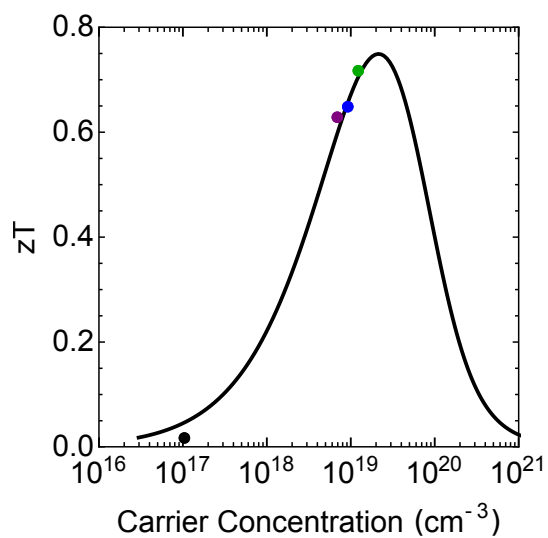


**Figure S5** The single parabolic band (SPB) model estimates that samples of  $K_{1-x}Ba_xAlSb_4$  exhibit nearly optimized carrier concentration. All phase pure samples agree well with SPB predictions.

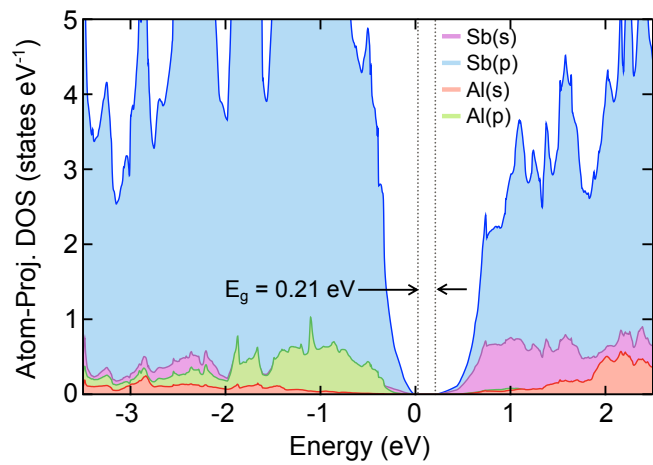


**Figure S6** Atom-projected density of states (DOS) of  $\text{KAlSb}_4$ . We find that the states near both band edges are dominated by antimony orbitals. The valence band has a weak contribution from aluminum  $p$  and  $s$  orbitals, whereas the conduction band is almost entirely determined by antimony states.